Chapter 9

Experimental studies

In the current chapter experimental studies of the ordinary reflectance and differential detector MO scanning microscopes are presented to verify the theoretical analysis presented in the previous chapters. In particular, the response using confocal pinhole sizes of varying size will be compared with theoretical predictions. The experimental results have been generated using an existing scanning laser microscope, the *x-y* SLM, which is described elsewhere [8,10,11,15]. However, a brief description of the operation and imaging capabilities of the *x - y* SLM will be presented in the current chapter.

In the previous analysis the theoretical response of the scanning microscopes were compared by analysing the step and impulse responses of the optical configurations investigated. However, it is difficult to generate the experimental impulse response of the scanning microscope due to problems associated with generating an object of truly infinitesimal extent. Hence, the following analysis concentrates on the investigation of the step response of the ordinary reflectance scanning microscope and differential detector MO scanning microscope. A series of experiments were performed to investigate the step response of the scanning microscope for a range of pinhole sizes. These are compared with theoretical results to determine the validity and accuracy of responses generated using the computational models developed.

9.1 The *x-y* scanning laser microscope, SLM

The *x-y* scanning laser microscope, SLM, has the ability to record magnetic domain structures which can be imaged using a variety of magneto-optic detection techniques and has been designed and constructed primarily for the study of magnetic thin films. The *x - y* SLM is also useful for observing non-magnetic contrast and hence, for

generating surface profile images of samples. The readout channel of the *x-y* SLM is analogous to that of the differential detector MO scanning microscope analysed previously, and is illustrated in Fig. 9.1.
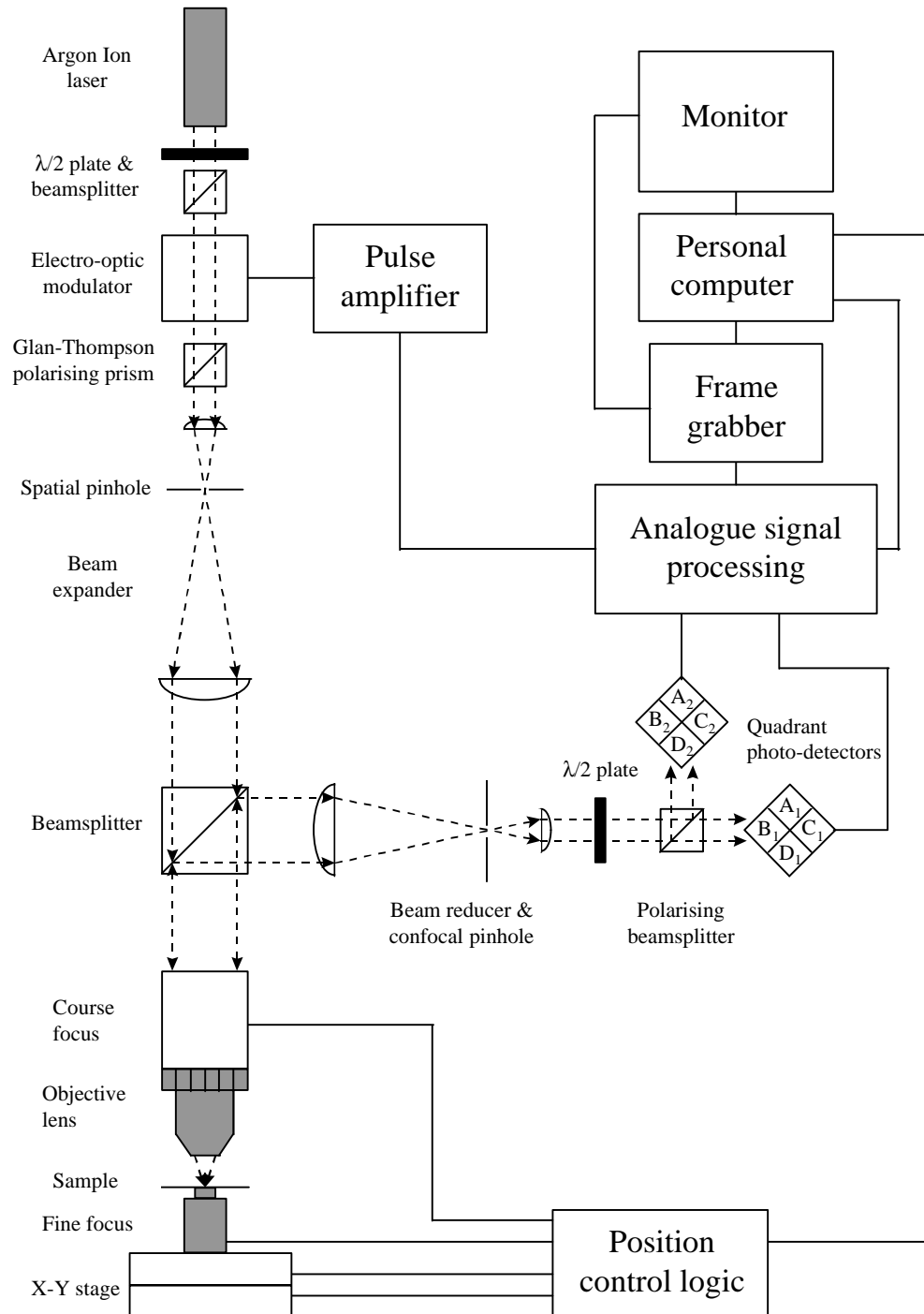

Figure 9.1 : *Block diagram of the x - y scanning laser microscope apparatus.*

A collimated, coherent light source is provided by a 5W (multiline) Argon Ion laser. The orientation of the first half-wave plate with respect to the polarising beamsplitter controls the amount of light which propagates through to the sample. The beam propagates through the electro-optic modulator which modulates the intensity of the beam at 300kHz, the Glan-Thompson polarising prism then determines the plane of polarisation of the beam incident on the sample. The beam expander and spatial pinhole expands the beam to form a clean Gaussian wavefront, such that $w_{e^{-2}} \approx 15mm$ at the back aperture of the objective lens, which is approximately 5mm in diameter. The beam then propagates through the infinity corrected microscope objective lens to form a diffraction limited spot on the surface of the sample.

Focusing of the objective lens is manually controlled using two piezo-electric stages. Coarse focusing is performed by adjusting the vertical position of the objective lens using the first piezo-electric stage and fine adjustment is performed by positioning the height of the sample using the second piezo-electric stage. The sample is mounted on a x - y stage which has linear encoders attached to enable controlled positioning of the stage to a precision of $0.1\mu m$ in either direction. The position control logic generates a reference signal which is used to synchronise the frame grabber with the position of the stage.

Upon reflection from the sample, the beam propagates to a beamsplitter which deflects the reflected beam towards the detection arm of the instrument. The beam reducer and confocal pinhole enables the reflected beam to cover the active area of the quadrant photo-detectors, and allows the instrument to be operated in the confocal mode. The half-wave plate and polarising beamsplitter arrangement is used to balance the light on the two-detectors when imaging magneto-optic contrast. At the polarising beamsplitter interface the reflected beam is split into its orthogonal x and y components which propagate towards the two quadrant photo-detectors. Eight signals are generated, one from each quadrant of the two photo-detectors, these are processed using the analogue signal processing electronics. The resulting signal is then passed into a slow-scan frame grabber where the image is stored prior to display on a colour monitor.

One of the advantages of the x - y SLM is its sensitivity to a wide variety of magnetic contrasts, i.e. polar Kerr, longitudinal Kerr, Faraday and magneto-optic phase contrast, and non-magnetic contrast. This is achieved by the judicious combination in the analogue signal processing electronics of the eight signals from the two quadrant photo-detectors.

For example, a total intensity, or reflectance, image is generated simply by adding together the eight signals from the two quadrant photo-detectors, i.e. $A_1+B_1+C_1+D_1+A_2+B_2+C_2+D_2$. Polar Kerr contrast is generated using the differential detection technique presented in this thesis, for which the difference between the total signal from the two quadrant photo-detectors is generated, i.e. $(A_1+B_1+C_1+D_1)-(A_2+B_2+C_2+D_2)$. This same combination can be used to generate Faraday contrast in transparent samples. However, the sample must be mounted on a reflecting mirror, since the x - y SLM only operates in reflectance.

9.2 Comparison of the experimental and theoretical step responses of the reflectance scanning microscope

The step response of the ordinary reflectance scanning microscope was generated by imaging the reflective edge of a commercial resolution test target etched into an aluminium coated glass slide [121]. Figure 9.2 illustrates the commercial test target used.
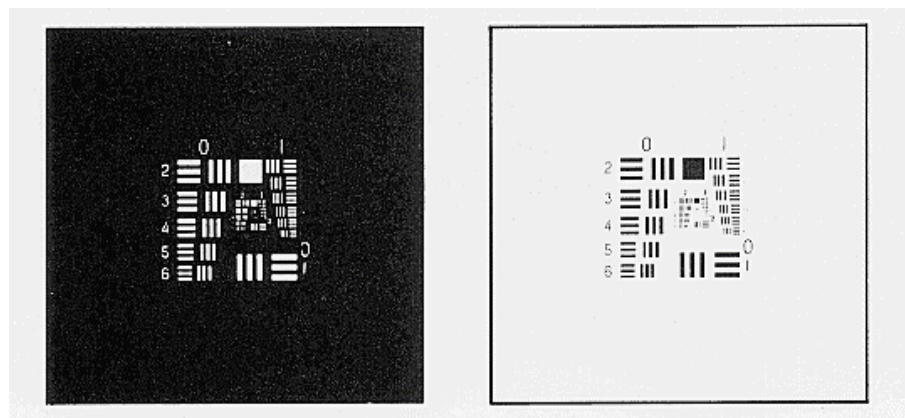

Figure 9.2 : *Commercial test target.*

The x - y SLM was configured for total intensity imaging and an image of the reflective edge was generated by scanning a 51.2µm x 51.2µm region along the reflective edge with a step size of 0.1µm (the smallest step size possible). Different scans of the same area were performed using four different confocal pinhole sizes : 25µm, 35µm, 50µm and 100µm. For a wavelength of 514nm and an auxiliary lens NA of 0.02, these pinhole diameters correspond to the values 0.9728, 1.3619, 1.9455 and 3.8911 in reduced optical units of λ/NA. Comparing these values with the plot of pinhole radius against impulse response FWHM, Fig. 6.11, it can be seen that employing the 25µm pinhole is the closest approximation to ideal confocal imaging, whereas employing the 100µm pinhole can be assumed to approximate to non confocal imaging.

The objective lens was brought into approximate focus by adjusting the vertical position of the objective lens using the coarse focusing system. A scan was then performed. However, during the course of each scan the height of the sample was adjusted in 2µm steps approximately every 70 scan lines, using the fine focusing system. This procedure was repeated for each scan such that the point where the objective lens was in perfect focus could be found easily. Figure 9.3 illustrates the four images generated using this technique.

Bright areas in Fig. 9.3 correspond to regions of low reflectance on the sample, and dark areas correspond to regions of high reflectance on the sample. Hence, scan lines where the greatest contrast is observed correspond to the point where the objective lens was in perfect focus. Thus, the responses along these scan lines can be assumed to represent the true, in-focus step response of the reflectance scanning microscope.

Figure 9.3 clearly illustrates the depth discrimination characteristics of the confocal optical system. In the case of the 25µm pinhole scan, Fig. 9.3(a), the SLM is very sensitive to the position of the focal plane, due to the depth discrimination properties of the confocal system. However, in the case of the 100µm pinhole scan, Fig. 9.3(d), which corresponds approximately to non-confocal imaging, the SLM is relatively insensitive to the amount of defocus.
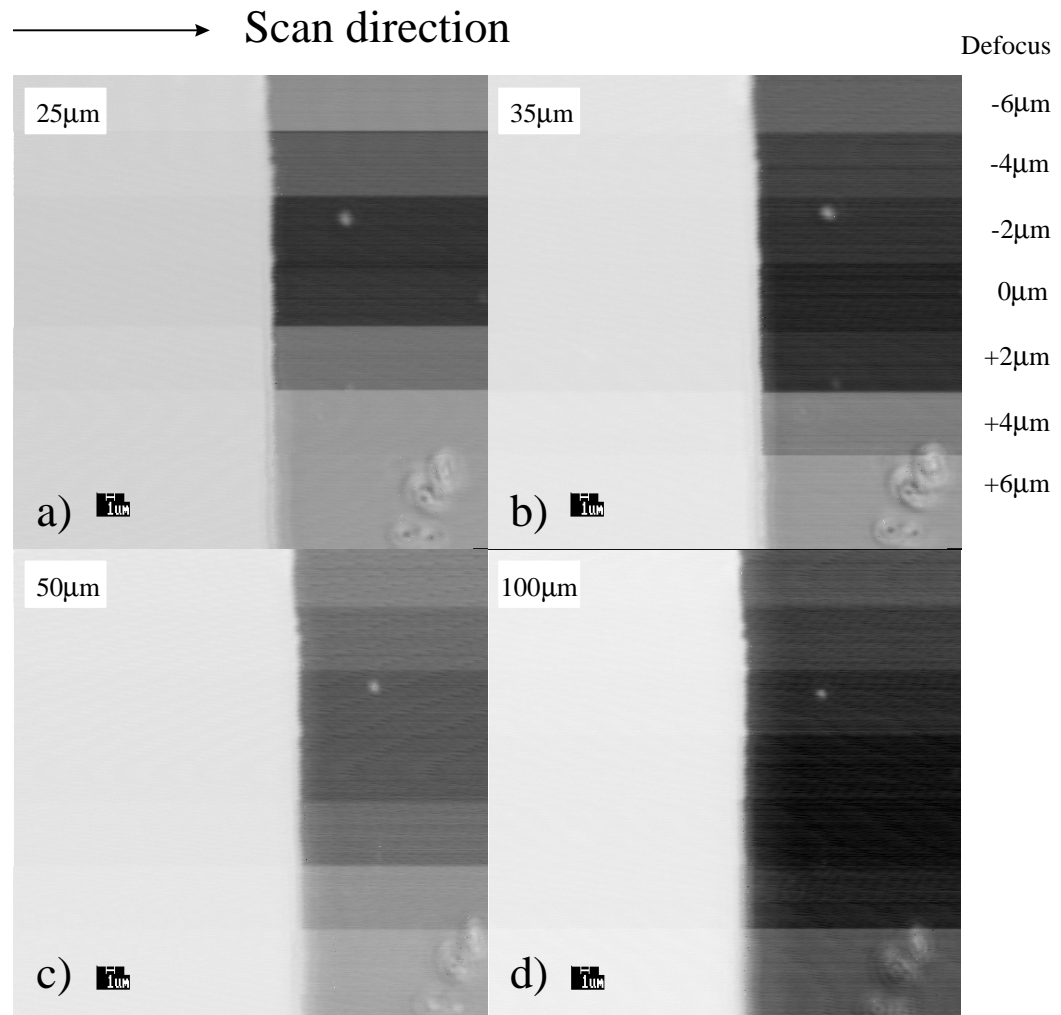
Figure 9.3 : *Total intensity scans (51.2μmx51μm) of a reflective edge generated using the x - y SLM for various confocal pinhole sizes and varying degrees of focus.*

Initial comparisons of the experimental and theoretical responses indicated that the slope of the theoretical prediction was too sharp in comparison with the experimental results. Hence, a high resolution surface profile image of the edge was acquired using a commercial Burleigh Personal Atomic Force Microscope (AFM), to investigate the quality of the edge. Figure 9.4 illustrates a plot of the surface characteristics of the edge.

The image of Fig. 9.4 shows the surface topography of the edge and not its reflectance properties. However, surface variations in the aluminium layer will introduce changes in the reflectance properties of the sample. In the theoretical analysis it is assumed that the edge is a perfect transition from 0% to 100%

reflectance in the scan direction, x, and extends to infinity in the orthogonal, y, direction. However, the edge clearly does not conform to such idealistic constraints. In some areas the edge is in fact sloping, i.e. the aluminium coating gets gradually thinner, over a 1μm region. If it is assumed that the sloping edge introduces a linear change in reflectance as the aluminium layer thins, then the edge may be modelled as a gradual change in reflectance over a 1μm interval. A more appropriate edge description, bearing in mind that the bare glass reflects a small amount of light and that aluminium is not a perfect reflector, might therefore be a sloped reflectance change from 20% to 80% over a 1μm distance.
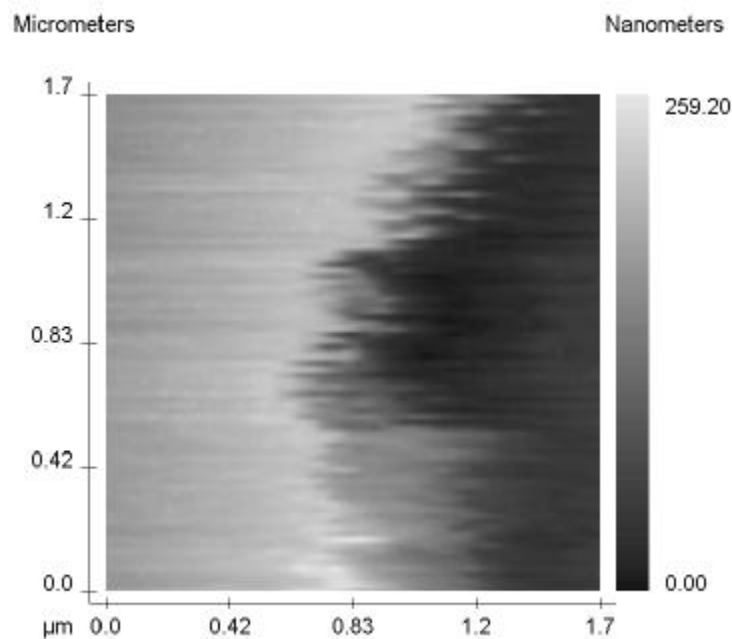
Figure 9.4 : *AFM image of the reflective edge.*

Figures 9.5 to 9.8 illustrate comparisons of normalised experimental steps, extracted from the images in Fig. 9.3, and theoretical step responses for the confocal reflectance scanning microscope employing the four sizes of confocal pinhole. The theoretical responses were generated using the transfer function approach where the apertures were assumed to be clear, aberration free, circular and of equal diameter under uniform incident illumination. The width of the Gaussian beam at the back aperture of the objective lens is measured to be $w_{e^{-2}} = 3r_{objective}$, hence, it is assumed that this truncated Gaussian distribution approximates to a uniform distribution.
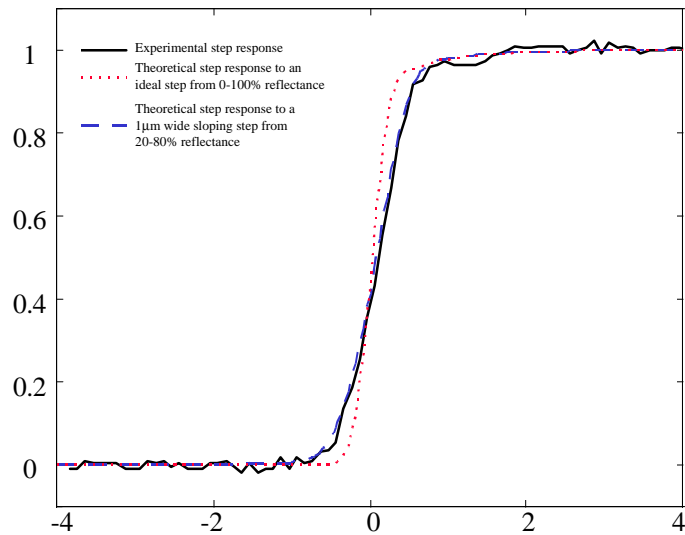
Figure 9.5 : *Experimental reflectance step response (solid line), theoretical reflectance step response to an ideal step from 0% to 100% reflectance (dotted line), theoretical reflectance step response to a slopping step 1mm wide (dashed) line, for a confocal pinhole diameter of 25mm.*
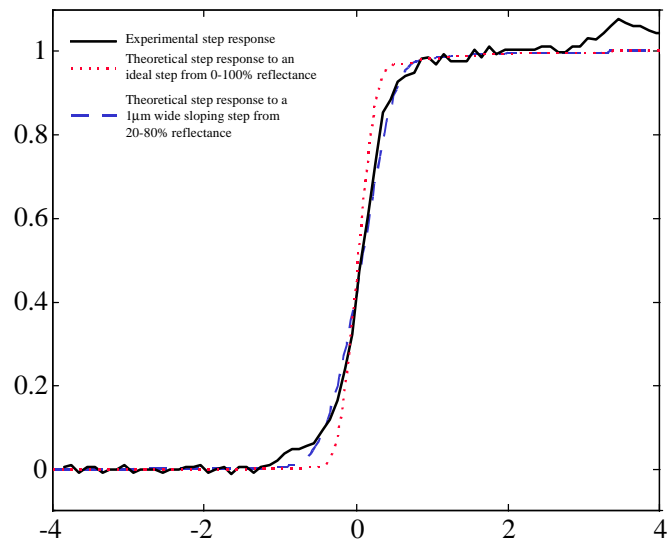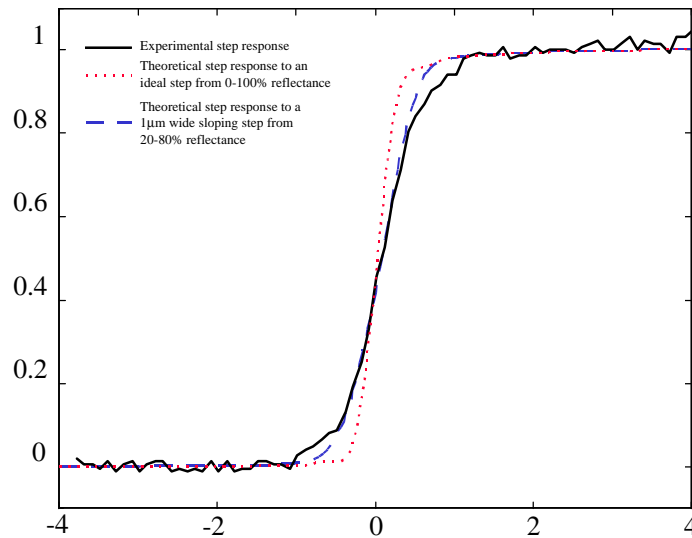

Figure 9.6 : *Experimental reflectance step response (solid line), theoretical reflectance step response to an ideal step from 0% to 100% reflectance (dotted line), theoretical reflectance step response to a slopping step 1mm wide (dashed) line, for a confocal pinhole diameter of 35mm.*
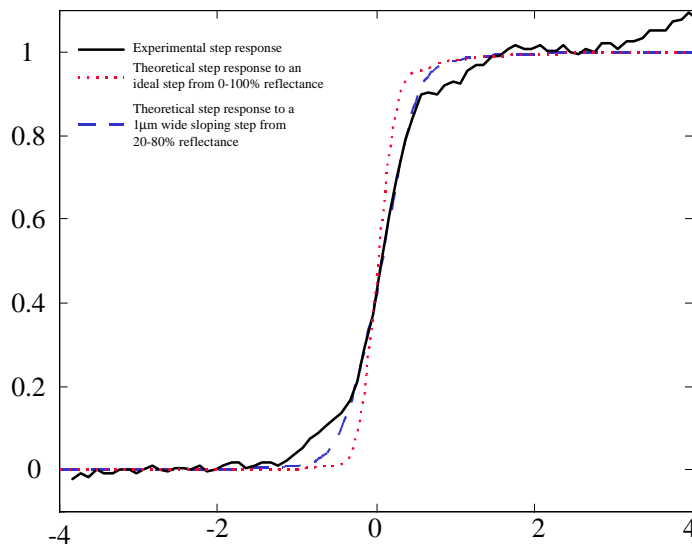
Figure 9.7 : *Experimental reflectance step response (solid line), theoretical reflectance step response to an ideal step from 0% to 100% reflectance (dotted line), theoretical reflectance step response to a slopping step 1**m**m wide (dashed) line, for a confocal pinhole diameter of 50**m**m.*

Figure 9.8 : *Experimental reflectance step response (solid line), theoretical reflectance step response to an ideal step from 0% to 100% reflectance (dotted line), theoretical reflectance step response to a slopping step 1**m**m wide (dashed) line, for a confocal pinhole diameter of 100**m**m.*

It is clear from Figs. 9.5 to 9.8 that the experimental results agree very closely within the range of the theoretical predictions. In the case of Figs. 9.5, 9.7 and 9.8 the slope of the experimental response agrees very closely with the theoretical response generated using the sloping step. Variations at the extremes of the response can be assumed to be due to surface variations on the sample and noise sources in the instrument. As observed by others, a smaller confocal pinhole size is seen to yield a sharper edge response [4].

9.3 Comparison of the experimental and theoretical step responses of the MO scanning microscope

To generate the differential detector MO step response the polar Kerr MO image of a magnetic bar structure was generated. The magnetic bar, of dimensions 100μm x 50μm, was recorded onto an erased Pt/Co multi-layer thin film, using the x - y SLM, with a write power of 10mW on the sample and a record field of 800Oe.

The x - y SLM was configured for differential detector polar Kerr imaging and an image of the magnetic edge was generated by scanning a 51.2μm x 51.2μm region area along the magnetic edge with a step size of 0.1μm, using an rms. laser power of 1mW at the surface of the sample. Different scans of the same area were performed using four different confocal pinhole sizes in the detection arm of the instrument : 25μm, 35μm, 50μm and 100μm. Prior to each scan the objective lens was brought into approximate focus using the coarse focusing system and the fine focus was adjusted until the maximum (peak to peak) Kerr signal was observed from the signal processing electronics. Figure 9.9 illustrates the four MO images generated using the x - y SLM.

Figure 9.9 clearly illustrates that unfortunately, like the reflectance edge, the magnetic edge is not ideal. The enlarged inset illustrates that there are relatively large areas of demagnetisation along the edge and 'worm like' features are evident along the step which are as a result of the low coercivity of the Pt/Co sample.
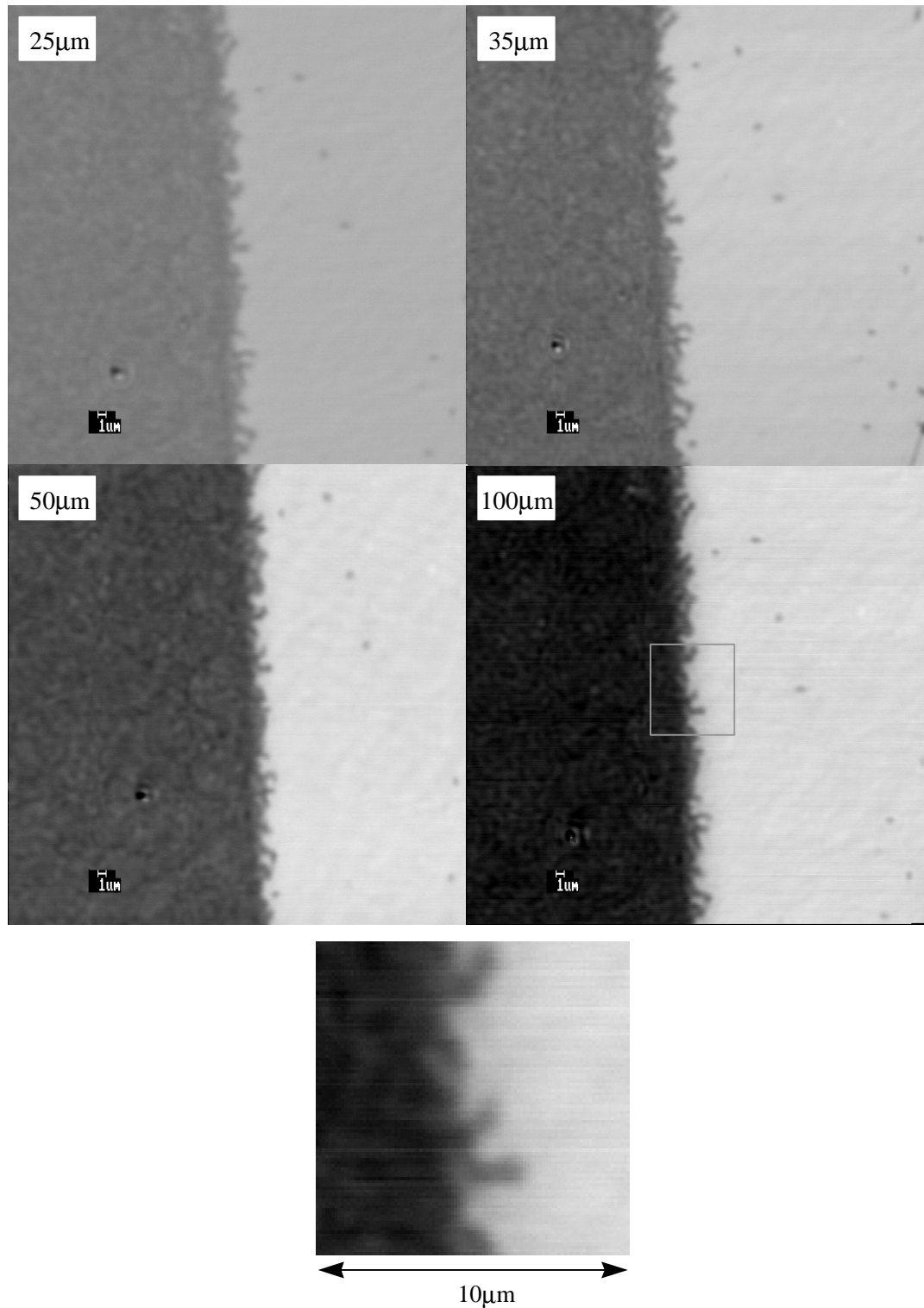
Figure 9.9 : *Magneto-optic polar Kerr scans (51.2**m**x51**m**m) of a magnetic edge generated using the x - y SLM, for various confocal pinhole sizes. Also illustrated is a magnified 10**m**m square region along the edge.*

Figure 9.10 illustrates a (DC) MFM image of a magnetic bit structure recorded on the same Pt/Co multi-layer film. Again, the 'worm-like' structure due to the demagnetised

regions around the edge is evident. This demonstrates that the demagnetised structure is due to the properties of the sample and not the imaging process. Hence, a problem encountered in the experimental analysis was acquiring a step response from the images in Fig. 9.9 without observing the demagnetised regions.
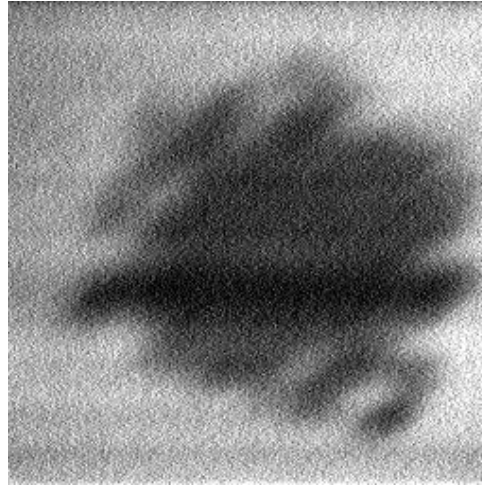

Figure 9.10 : *Experimental DC-MFM image of a magnetic bit structure recorded in a Pt/Co multi-layer sample; scan 5μmx5μm.*

Figures 9.11 to 9.14 illustrate comparisons of normalised experimental steps, extracted from the images in Fig. 9.9, and theoretical step responses for the confocal differential detector MO scanning microscope employing the four sizes of confocal pinhole. The theoretical responses were generated using the transfer function approach where the apertures were assumed to be clear, aberration free, circular and of equal diameter under uniform incident illumination.

The responses of Figures 9.11 to 9.14 illustrate that the demagnetised regions along do appear the magnetic edge extracted from the experimental step response. However, the Figures clearly illustrate that the slope of the theoretical predictions agree extremely well with the experimental results.

It is discussed in sec. 6.4.3 that theoretical predictions indicate that the response of the differential detector MO scanning microscope is unaffected by the introduction of a confocal pinhole in the detection arm of the instrument and that the confocal mode of operation offers no resolution enhancement over the non confocal optical system.
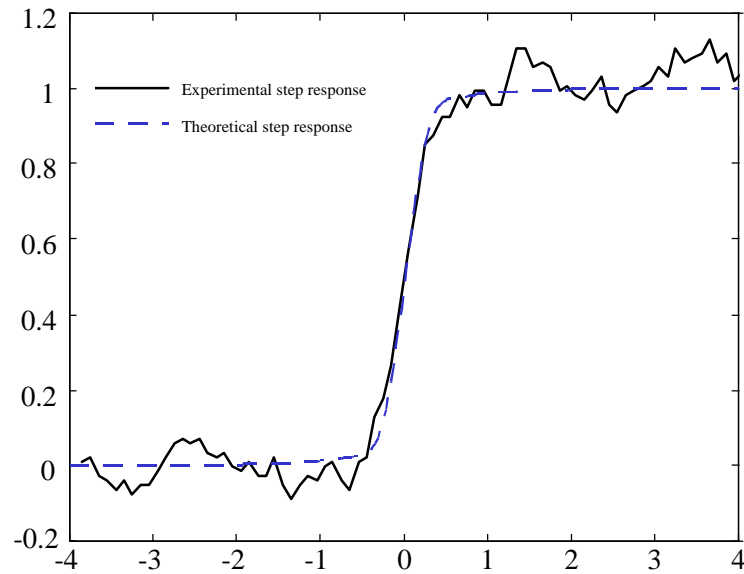
Figure 9.11 : *Experimental step response (solid line), theoretical differential detector MO step response to an ideal step from -0.5° to +0.5° Kerr rotation (dotted line) for a confocal pinhole diameter of 25mm.*

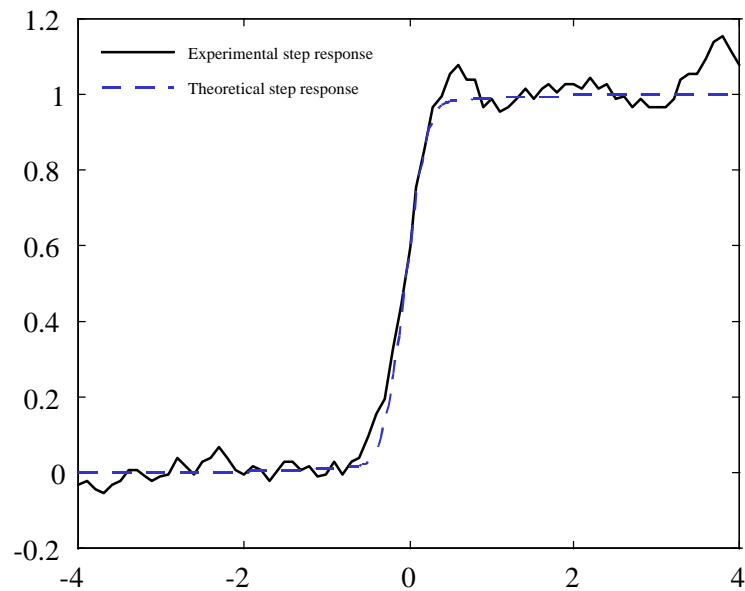**Figure 9.12 :** *Experimental step response (solid line), theoretical differential detector MO step response to an ideal step from -0.5° to +0.5° Kerr rotation (dotted line) for a confocal pinhole diameter of 35mm.*
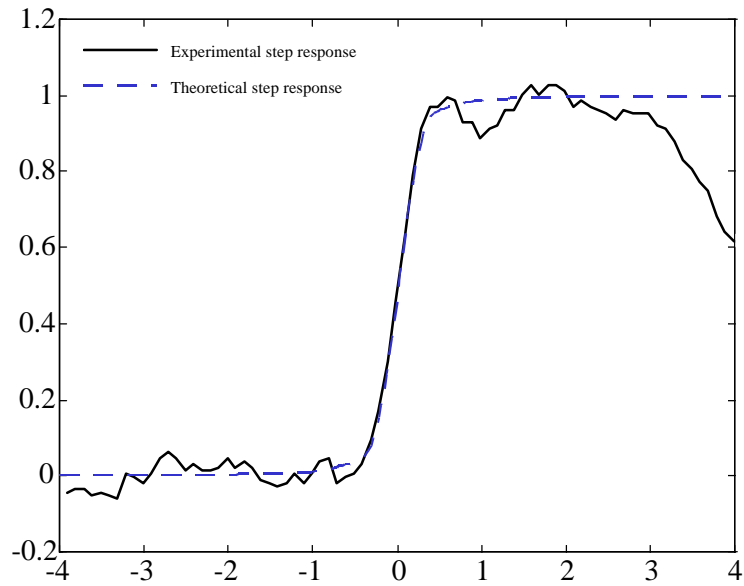
Figure 9.13 : *Experimental step response (solid line), theoretical differential detector MO step response to an ideal step from -0.5° to +0.5° Kerr rotation (dotted line) for a confocal pinhole diameter of 50mm.*
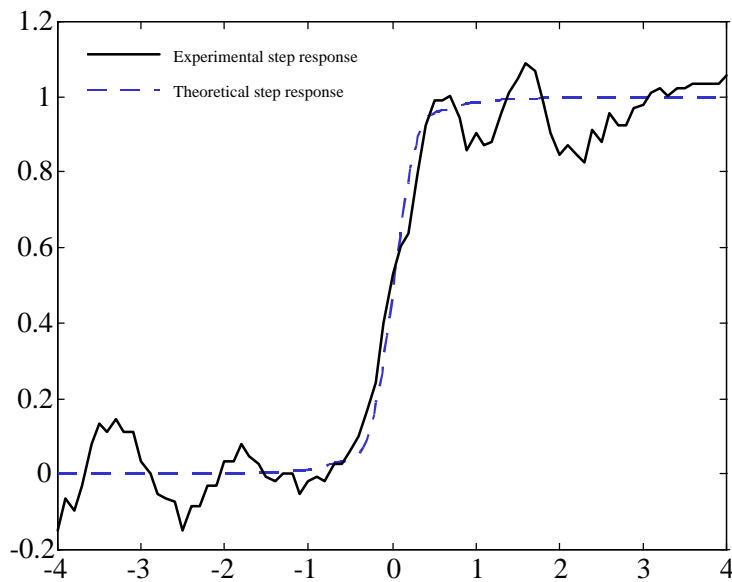

Figure 9.14 : *Experimental step response (solid line), theoretical differential detector MO step response to an ideal step from -0.5° to +0.5° Kerr rotation (dotted line) for a confocal pinhole diameter of 100mm.*

The plot of pinhole radius against impulse response FWHM, Figure 6.20, illustrates that the FWHM of the impulse response changes very little as the size of the confocal pinhole is varied. Thus, the slope of the step response remains unaffected. Since the results in Figures 9.11 to 9.14 illustrate that the experimental results agree with the theoretical predictions, then it can be safe to assume that the experimental results confirm the theoretical predictions that the confocal mode of operation for the differential detector MO scanning microscope offers no enhanced lateral resolution improvements over the Type 1 configuration.

Figures 9.15 and 9.16 illustrates polar Kerr images of a data pattern which has been recorded onto a Pt/Co multi-layer sample. The scans were acquired using the same procedure used for generating the responses in Fig. 9.9. The image of Fig. 9.15 was taken using a confocal pinhole size of 25μm and the image of Fig. 9.16 was taken using a confocal pinhole size of 100μm. The power at the sample was maintained at 1mW for both scans. The enlarged insets in both Figs. 9.15 and 9.16 illustrate the same bit structure taken from the two images.

The two responses through the centre of the bit structure illustrated in the enlarged insets of Figs. 9.15 and 9.16 were extracted, normalised and plotted against each other, as illustrated in Fig. 9.17.

Figure 9.17 clearly illustrates that the gradient along the rising and falling slopes of the responses is identical for the two cases. However, at the extremes of the responses, i.e. at the top and bottom of the steps, the responses do differ. Figure 9.18 illustrates the theoretical step response of the differential detector MO scanning microscope to a magnetic edge for confocal pinhole sizes of 25μm and 100μm. As expected from previous results, the slope of the two responses along the edge is identical. However, at the extremes of the theoretical step responses the predictions do differ, as was observed experimentally. Again, the experimental results indicate that the introduction of a confocal pinhole in the differential detector MO system does not improve the lateral resolution of the scanning microscope.
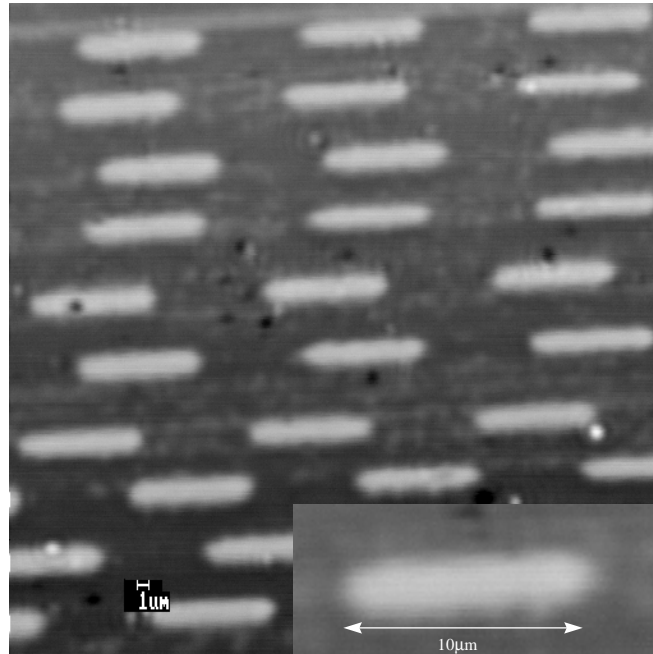
Figure 9.15 : *Magneto-optic polar Kerr scans (51.2μmx51μm) of recorded bits generated using the x - y SLM with a confocal pinhole diameter of 25μm.*
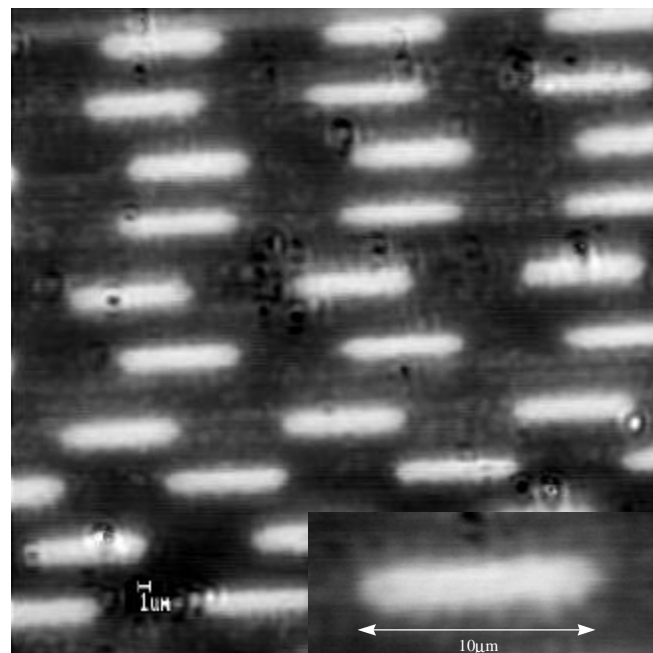

Figure 9.16 : *Magneto-optic polar Kerr scans (51.2μmx51μm) of recorded bits generated using the x - y SLM with a confocal pinhole diameter of 100μm.*
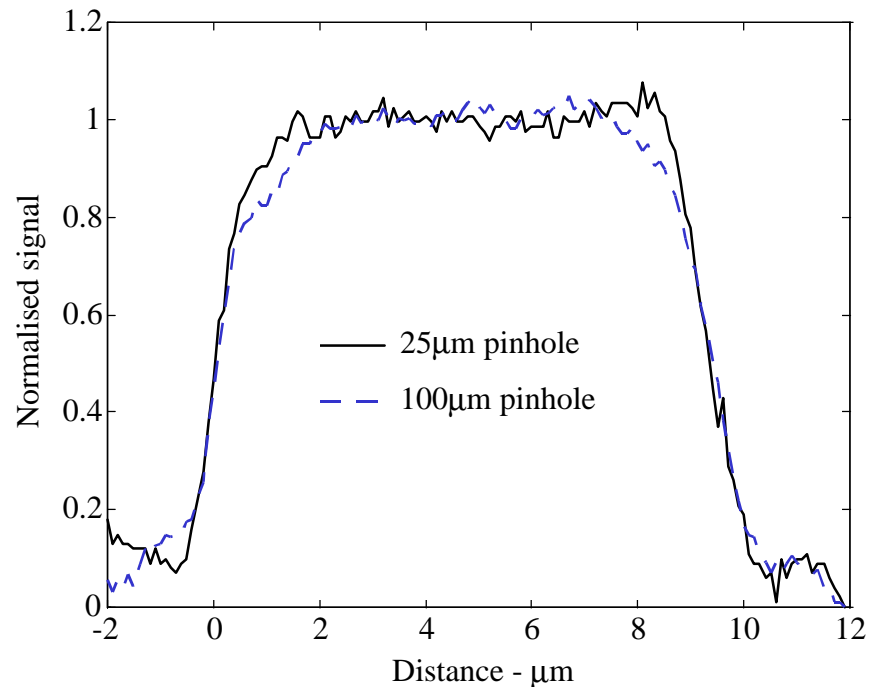
Figure 9.17 : *Polar Kerr responses of a recorded bit generated using the x - y SLM with a confocal pinhole diameter of 25**m**m (solid line) and 100**m**m (dashed line).*
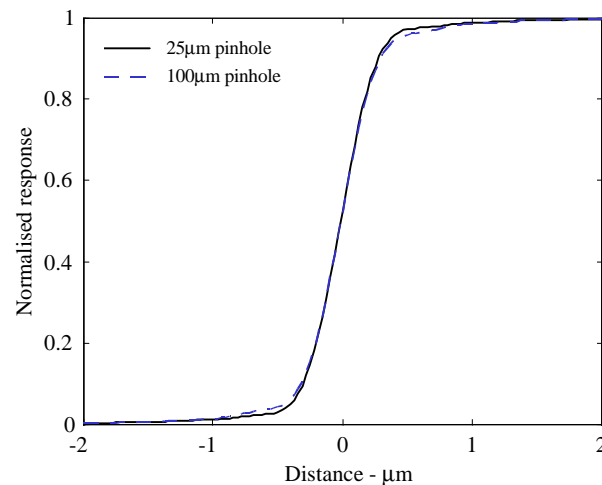

Figure 9.18 : *Theoretical MO Kerr step response, generated using the direct calculation approach with confocal pinhole diameters of 25**m**m (solid line) and 100**m**m (dashed line).*

Hence, using experimental analysis the step response of both the reflectance and differential detector MO scanning microscope has been investigated and compared with theoretical predictions. In particular, the role of confocal pinhole size on the

response of the scanning microscopes was investigated. In the analysis of the reflectance system it was found that the theoretical and experimental results agree extremely well, and it can be clearly assumed that the theoretical models produce accurate responses. In the differential detector MO analysis comparisons seem to indicate that again the results agree very well. An interesting discovery being that the confocal differential detector MO scanning microscope does not offer enhanced lateral resolution properties over the non-confocal system, a result that was deduced using the theoretical analysis.

Previously published experimental results have in fact indicated that confocal imaging with a differential MO configuration does improve resolution [11,49]. However, in light of the work of this thesis it is most probable that a systematic error was introduced during the focus set up procedure in the previous work. When generating the previous results [11,49] it was assumed that the objective lens was in perfect focus when a clear Gaussian irradiance distribution was observed on the quadrant photo-detectors [122]. However, careful analysis has shown that the irradiance distribution will change depending upon the size of the confocal pinhole. Figure 9.19 illustrates the predicted irradiance plots of the incident field distribution observed on the quadrant photo-detector for varying sizes of confocal pinhole size. Such distributions were also observed experimentally. Thus, it can be clearly seen that the irradiance distribution is not always Gaussian, as assumed.

It should be noted that for more accurate and precise quantitative comparisons to be made between theoretical and experimental results then better samples must be used. The sample used in this exercise did not offer the perfect edge which was required by the theoretical analysis, thus, introducing uncertainties into the experimental results. It is recommended that in any future work experimental observations should be made using samples which offers more idealistic characteristics, as required by the theoretical modelling process.
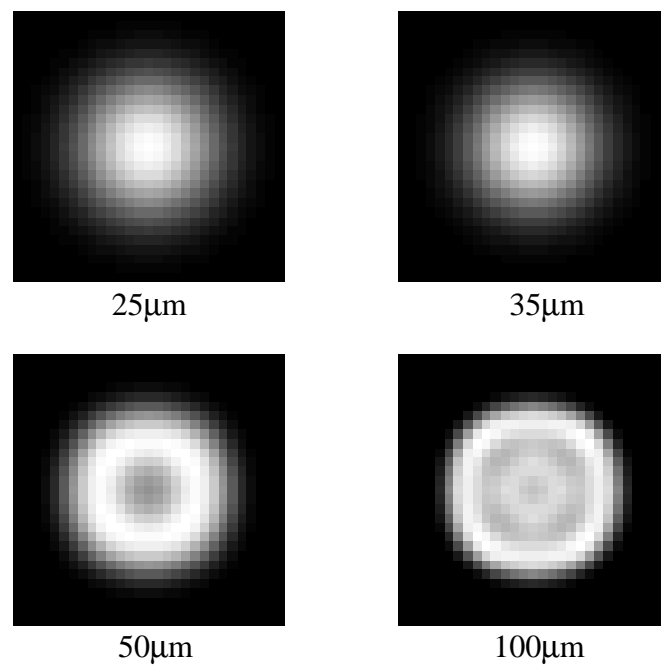
25μm   35μm

50μm   100μm

Figure 9.19 : *Irradiance plots of the incident field distribution observed on the quadrant photo-detector for varying sizes of confocal pinhole size.*